Title

Therapeutic targeting of tumor hypoxia and necrosis with antibody α-radioconjugates

Journal

Antibody Therapeutics, 1(2)

ISSN

2516-4236

Authors

Lopez, Tyler
Ramirez, Aaron
Benitez, Chris
et al.

Publication Date

2018-09-17

DOI

10.1093/abt/tby010

Peer reviewed

Antibody Therapeutics, 2018, Vol. 1, No. 2 ***55–63***
doi:10.1093/abt/tby008
Advance Access Publication on 05 October 2018

Method articles

Selectivity Conversion of Protease Inhibitory Antibodies

Tyler Lopez, Aaron Ramirez, Chris Benitez, Zahid Mustafa, Henry Pham, Ramon Sanchez and Xin Ge*

Department of Chemical and Environmental Engineering, Bourns College of Engineering, University of California Riverside, Riverside, CA 92521, USA

Received: July 20, 2018; Revised: September 19, 2018; Accepted: September 25, 2018

ABSTRACT

Background: Proteases are one of the largest pharmaceutical targets for drug developments. Their dysregulations result in a wide variety of diseases. Because proteolytic networks usually consist of protease family members that share high structural and catalytic homology, distinguishing them using small molecule inhibitors is often challenging. To achieve specific inhibition, this study described a novel approach for the generation of protease inhibitory antibodies. As a proof of concept, we aimed to convert a matrix metalloproteinase (MMP)-14 specific inhibitor to MMP-9 specific inhibitory antibodies with high selectivity.

Methods: An error-prone single-chain Fv (scFv) library of an MMP-14 inhibitor 3A2 was generated for yeast surface display. A dual-color competitive FACS was developed for selection on MMP-9 catalytic domain (cdMMP-9) and counter-selection on cdMMP-14 simultaneously, which were fused/conjugated with different fluorophores. Isolated MMP-9 inhibitory scFvs were biochemically characterized by inhibition assays on MMP-2/-9/-12/-14, proteolytic stability tests, inhibition mode determination, competitive ELISA with TIMP-2 (a native inhibitor of MMPs), and paratope mutagenesis assays.

Results: We converted an MMP-14 specific inhibitor 3A2 into a panel of MMP-9 specific inhibitory antibodies with dramatic selectivity shifts of 690–4,500 folds. Isolated scFvs inhibited cdMMP-9 at nM potency with high selectivity over MMP-2/-12/-14 and exhibited decent proteolytic stability. Biochemical characterizations revealed that these scFvs were competitive inhibitors binding to cdMMP-9 near its reaction cleft via their CDR-H3s.

Conclusions: This study developed a novel approach able to convert the selectivity of inhibitory antibodies among closely related protease family members. This methodology can be directly applied for mAbs inhibiting many proteases of biomedical importance.

Statement of Significance: To achieve high selectivity required for therapies, we developed a novel approach for the generation of protease inhibitory antibodies with nM potency and decent proteolytic stability. The methodology demonstrated here can be readily applied to many proteases of biomedical importance.

KEYWORDS: protease; inhibitory antibody; MMP; FACS; selectivity

INTRODUCTION

Accounting for roughly 2% of human genome, proteases are important signaling molecules precisely controlling a wide variety of physiological processes. Consequently, many diseases are associated with altered protease expression or substrate proteolysis [1–4]. It has been estimated that 5–10% of all pharmaceutical targets for drug

*To whom correspondence should be addressed. Xin Ge. Tel: 951-827-6229; Fax: 951-827-5696; Web: gelab.ucr.edu; Email: xge@engr.ucr.edu

developments are proteases [5]. Among 569 human proteases identified, 279 (49%) are extracellular or pericellular enzymes (121 metalloproteinases, 138 serine, 6 threonine, 5 cysteine, and 9 aspartic proteases), and thus accessible to therapeutic antibodies [6]. Some well-characterized druggable proteases include cathepsin B, which promotes tumor growth, metastasis, and angiogenesis through its proteolytic cascades [7]; cysteine protease falcipain 1, which is required for malaria to invade host cells [8, 9]; matrix metalloproteinases (MMPs), which cause wound healing delays due to excessive matrix degradation [10]; thrombin and factor XIa, whose dysregulated activities are responsible for blood coagulation [11]; and plasma kallikrein, whose upregulation due to genetic deficiency of serpin C1-inhibitor leads to hereditary angioedema [12]. One therapeutic strategy is to block these abnormal or pathogenic proteolysis by inhibiting their catalytic reactions.

Most therapeutic protease inhibitors currently in clinical use or under developments are chemical compounds or peptide mimics derived from their substrates [2, 5]. Considering the vast proteolytic landscape and the levels of protease complexity [3, 13], specificity is highly desired for any protease inhibition therapy. However, achieving target specificity can be challenging because proteolytic pathways often consist of highly homologous family members that share the same domain folding and catalytic chemistry [14]. The crucial importance of specificity has been highlighted by the extensive studies on inhibition of MMPs using zinc-chelating compounds as a strategy for treating cancer [15, 16]. Although pre-clinical results were promising, previous attempts focusing on the development of broad-spectrum chemical compound inhibitors, e.g. hydroxamates, all failed in clinical trials due to lack of efficacy and severe side effects caused by non-specific inhibition of other metalloproteinases [17, 18].

Our studies [19–21], consistent with others [22–31], have demonstrated the feasibility of monoclonal antibodies (mAbs) to act as highly potent and highly selective inhibitors of secreted or cell surface proteases. However, even with recent technology advancements such as epitope synthetic mimicry [26], competitive phage elution [25], convex paratope design [19], and epitope-specific FACS [32], the discovery of protease inhibitory mAbs still presents a challenge in general. This is largely because the isolated antibodies need to not only specifically bind, but also efficiently inhibit the protease of interest. This study aims to develop a novel approach for the generation of protease inhibitory antibodies by engineering an active site inhibitor and steering its selectivity toward a new target. As a proof of concept, we started with an MMP-14 specific inhibitor single-chain Fv (scFv) 3A2 and changed its specificity toward MMP-9, which is an important collagenase associated with maladies such as neuropathic pain [33]. We hypothesize that affinity maturation using yeast surface display and competitive FACS can achieve this selectivity conversion. Our underlying rationale is that antibody affinity and its selectivity are correlated [34–36], i.e. perfect shape complementarity and strong interaction are the factors leading to both high-affinity binding and high-selectivity inhibition. By incubating 3A2 random mutagenesis library cells with MMP-9 and MMP-14 conjugated/fused with different fluorophores simultaneously, dual-color competitive FACS can in principle isolate antibodies either mono-specific to MMP-14 or MMP-9 or bi-specific to both (Fig. 1). This study mainly focuses on mono-specific MMP inhibitors, especially on changing 3A2's specificity from MMP-14 to MMP-9. The beneficial effects on enhanced proteolytic stability will also be studied.

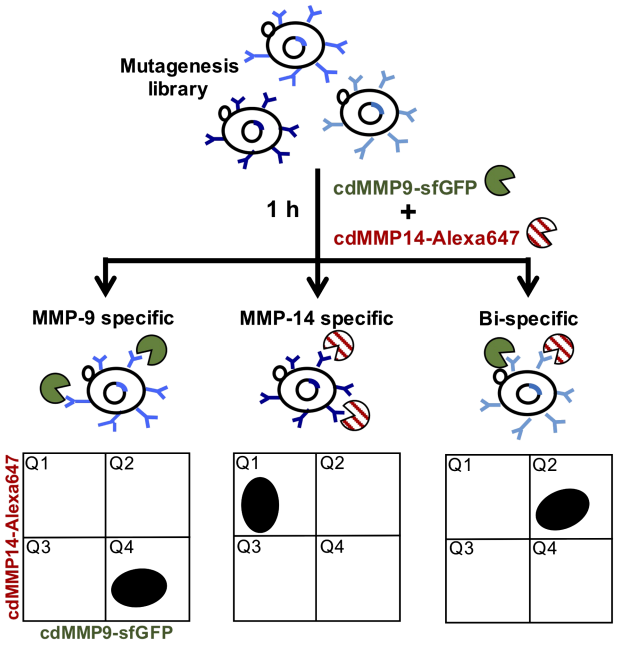

Figure 1. Scheme for specificity screening by competitive FACS. Random mutagenesis library of 3A2 scFv was displayed on yeast cell surface and co-incubated with cdMMP9-sfGFP and cdMMP14-Alexa647, allowing the isolation of inhibitory antibodies either mono-specific to cdMMP-9 or cdMMP-14 or bi-specific to both.

MATERIALS AND METHODS

3A2 error-prone scFv yeast display

To achieve efficient yeast surface display and FACS, V_H and V_L genes of Fab 3A2 were amplified and its scFv gene was assembled by overlapping polymerase chain reaction (PCR). Error-prone mutagenesis of 3A2 scFv was generated using Taq DNA polymerase with 120-μM dATP, 100-μM dCTP, 360-μM dGTP, 2.5-mM dTTP, 5-μg/mL BSA, 3.28-mM $MgCl_2$, and 0.5-mM $MnCl_2$. Primers were designed to be 28–30 nt with T_m of 63°C and GC contents of 55–60%. The mutation product was cloned into the yeast display plasmid pCTCon2 and transformed into *Saccharomyces cerevisiae* competent cells. The library size was based on serial dilution. The mutation rate was determined by Sanger sequencing results of randomly picked clones. A total of 5×10^9 cells of the constructed library were cultured on SD/-Trp/-Ura/penicillin–streptomycin agar plates at 30°C for 48 h. Thirty OD_{600} of cultured cells were inoculated into 600 mL of SD/-Trp/-Ura and incubated at 30°C with 250 rpm shaking for 12 h. Cells were then collected by centrifugation at 6,000 × g for 2 min, and 8 OD_{600} cells were further

cultured for scFv expression in 20-mL yeast nitrogen base-Trp/-Ura drop-out medium supplemented with 5 mL of 20% galactose at room temperature with 250 rpm shaking for 48 h.

FACS

For fluorescence labeling, superfolder GFP (sfGFP) was cloned at the C-terminal of catalytic domain (cd) of MMP-9. cdMMP9-sfGFP was periplasmically expressed in *Escherichia coli* and purified using an Ni-NTA column (Qiagen). cdMMP-14 was produced as previously described [37] and chemically conjugated with Alexa-647 (Invitrogen). Enzymatic activities of both MMPs were confirmed. In the first round of sorting (R1), 4 OD_{600} of cultured library cells were incubated with 600 µL of 800-nM cdMMP9-sfGFP in darkness for 1 h. After three washes with assay buffer (50-mM Tris–HCl pH 7.5, 150-mM NaCl, 5-mM $CaCl_2$, 2.0-mM $ZnCl_2$), cells were suspended in 4-mL assay buffer for FACS. A sample of the EBY100 host was labeled the same way as the negative control. Cells were sorted on a BioRad Se3 flow cytometer equipped with 488/640-nm lasers. Filters FL1 (526/48 nm) and FL3 (615/25 nm) were used for cdMMP9-sfGFP and cdMMP14-Alexa647, respectively. The forward and side scatter voltages were set at 317v and 341v with a threshold of 5. A triangle gate was used to select the top portion of GFP positive cells while excluding the clones showing high Alexa-647 signals. Isolated cells were plated on a SD/-Trp/-Ura/penicillin–streptomycin agar plate for growth at 30°C for 48 h after which the cells were collected in 20% glycerol SD/-Trp/-Ura media and stored at −80°C. In R2-R4, cells covering 10× the library diversity of previous round were cultured and labeled with preset concentrations of cdMMP9-sfGFP and cdMMP14-Alexa647. Colonies were randomly picked after R4 for monoclonal FACS screening, in which cells were labeled with 400-nM cdMMP9-sfGFP and 400-nM cdMMP14-Alexa647. Both scanning and sorting were performed at a rate of 2,000 events/s with a mild agitation to prevent the cells from settling.

Biochemical characterizations

Plasmids of the isolated clones were extracted using Zymoprep yeast plasmid kit (Zymo). scFv fragments of isolated clones and their site-directed mutants were cloned into pMoPac for *E. coli* periplasmic expression [38] and purified by Ni-NTA chromatography. Binding kinetics of purified scFvs were measured by biolayer interferometry using BLItz (ForteBio) on streptavidin biosensors coated with cdMMP-9 which had been previously biotinylated using EZ-Link Sulfo-NHS-LC biotinylation kit (Thermo Fisher). The determined k_{on} and k_{off} parameters were used to calculate the K_D values. Inhibition assays were performed by reacting serially diluted scFvs with 10-nM cdMMP-9 for 30 min, and the remaining activity of cdMMP-9 was measured with 1-µM M2350 peptide substrate (Bachem). The fluorescence was monitored with excitation and emission wavelengths at 325 and 392 nm using a spectrophotometer (BioTek). The inhibition potency of the scFvs K_i was calculated using equation $K_I = IC_{50}/(S/K_m + 1)$ [39]. Inhibition mode was determined by establishing Lineweaver–Burk plots at different scFv concentrations. cdMMP-12 mutation was designed using PROSS algorithm [40] and produced in the periplasmic space of *E. coli* for inhibition specificity tests. Recombinant human MMP-2 was obtained from Anaspec. The enzymatic activities of both cdMMP-12 and MMP-2 were tested. In competitive ELISA, Maxisorp microplates (Thermo Scientific) were coated with 4-µg/mL cdMMP-9 and blocked with skim milk. After washing, the plates were incubated with scFv at its affinity concentration for 1 h and washed again. 4 µM to 3 nM of the N-terminal domain of TIMP-2 (nTIMP-2), prepared as previously described [41], was then added and incubated for 1 h to compete with the scFv for binding on immobilized cdMMP-9. Anti-cMyc-HRP was then added to detect captured scFvs and the signals were developed using TMB substrate (Thermo Fisher). For *in vitro* stability tests, 1-µM purified scFvs were incubated with 1-µM cdMMP-9 in assay buffer at 37°C for 3 or 12 h. Densitometric analysis of scFv bands (30 kDa) on SDS-PAGE was performed using Image Lab (Bio-Rad). To reduce errors from variations in staining and destaining, gel background for each band was quantified and subtracted.

RESULTS

MMP homology analysis

The objective of this study is to test the feasibility of converting the inhibition selectivity of an antibody between closely related protease family members. As a proof of concept, we aimed to generate MMP-9 specific inhibitory antibodies by engineering an MMP-14 inhibitor. As zinc-dependent endopeptidases, catalytic domains of human MMPs possess a homologous protein folding with highly conserved secondary structures (Fig. 2A). Amino acid sequence comparison of cdMMP-2/-9/-12/-14 reveals that they share 47–60% identity and 56–67% similarity (Table S1). The major structural differences occur in the loop regions, while the variations in surface charge and topology around their well-pronounced catalytic clefts are relatively subtle (Fig. 2B). Encouraged by the exclusive specificity usually offered by mAbs, we hypothesized that mAb inhibitors can distinguish between closely related MMP family members with high selectivity.

3A2 scFv surface display and mutagenesis library construction

MMP-14 specific inhibitory Fabs were previously isolated from synthetic antibody libraries [19]. Particularly, Fab 3A2 exhibited single digit nM affinity/potency toward cdMMP-14 without significant inhibitory functions on other MMPs at µM concentrations. To convert the inhibitory selectivity of 3A2 using dual-color competitive FACS, scFv antibody fragment was chosen because this well-documented format has been very successful for yeast surface display [42]. The gene of scFv 3A2 (V_H-GS linker-V_L) was assembled and fused to the C-terminus of the a-agglutinin mating protein Aga2p subunit, and the fusion protein was expressed

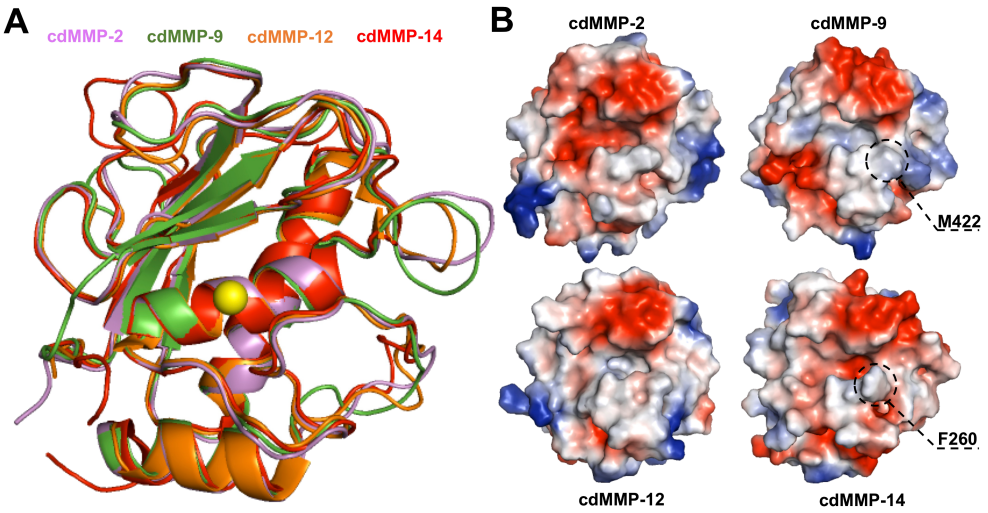

Figure 2. Superimpose of catalytic domains of MMP-2 (purple, 1QIB), -9 (green, 1GKD), -12 (orange, 1JK3) and -14 (red, 1BQQ) shown as (A) cartoon and (B) surface charge. cdMMPs share highly conserved overall protein folding, secondary structure backbones and catalytic zinc (yellow sphere). The catalytic clefts are well pronounced with subtle differences on surface topology and charges. Extruded Phe260 on cdMMP-14 and relatively flat Met422 on cdMMP-9 are circled.

in *S. cerevisiae* EBY100. Surface display of scFv 3A2 wt was examined by FACS after cells were concurrently incubated with 400-nM cdMMP9-superfolderGFP (sfGFP, [43]) fusion protein and 400-nM cdMMP14 conjugated with Alexa-647. FACS results indicated that the cells expressing Aga2p-3A2 showed a mean fluorescence signal of 97 on cdMMP14-Alexa647 (Fig. 3), significantly higher than that of host cells EBY100 without scFv expression (mean = 4.2), suggesting successful display of active scFv 3A2 on yeast cell surface. In addition, the fluorescence signals on cdMMP9-sfGFP showed no difference between 3A2 or the host, indicating that 3A2 was selective without cross reaction with cdMMP-9, consistent with our previous observations [19].

Cloning error-prone mutagenesis product of scFv 3A2 gene into the yeast surface display vector resulted in 4.5×10^8 *E. coli* colonies. DNA sequencing 20 randomly picked clones indicated 5.2 mutations on average per gene across the entire scFv sequence, equivalent to a 1.9% mutation rate. Transforming EBY100 competent cells with scFv 3A2 mutagenesis plasmids generated a library with a size of 2×10^7 mutants. Library cells were cultured and induced with 4% galactose for scFv expression then stained with 400-nM cdMMP9-sfGFP and 400-nM cdMMP14-Alexa647. FACS analysis revealed that the histogram of fluorescence signal associated with MMP-9 was widened with a mean of 22 (Fig. 3). This value was higher than that of host cells or the cells displaying scFv 3A2 (stained in the same manner), implying that the constructed library had the potential to isolate clones with high affinities on cdMMP-9.

Competitive FACS for cdMMP-9 positive clones

To isolate scFvs specific to cdMMP-9 without cross reaction with cdMMP-14, library cells were labeled with various concentrations of cdMMP9-sfGFP and cdMMP14-Alexa647 and sorted for cdMMP-9^{high} and cdMMP-14^{low} clones by four rounds of FACS. Considering that wt 3A2 scFv weakly bound to cdMMP-9 with an affinity >5 μM, in the first round of sorting, 30 million scFv library cells were incubated with a high concentration of cdMMP9-sfGFP at 800 nM for 1 h and the top 5% (1.5×10^6 cells) of GFP-positive cells were selected to recover any cdMMP-9 binders. In R2, to achieve selectivity, competitive incubation was introduced by labeling library cells with 800-nM cdMMP9-sfGFP and 800-nM cdMMP14-Alexa647 simultaneously. A total of 20 million cells were sorted, and on FACS 2-D histogram, a triangle gate was set to select the top 1% (2×10^5 cells) of cdMMP9-sfGFP positive cells while excluding the ones with a high cdMMP14-Alexa647 signal. To isolate scFv clones with improved binding affinity and selectivity, in R3 and R4, more stringent concentrations of cdMMP9-sfGFP were used at 400 nM and 200 nM, respectively, while maintaining the competitor cdMMP14-Alexa647 concentration at 800 nM. A total of 20 and 10 million cells were sorted in R3 and R4 with the selection gates tightened to be 1% and 0.5% of cdMMP9-sfGFP^{high} and cdMMP9-Alexa647^{low} population, resulting in 2×10^5 and 5×10^4 cells collected from R3 and R4, respectively. FACS analysis on the post-sort populations for each round (stained with 400-nM cdMMP9-sfGFP and 400-nM cdMMP14-Alexa647) revealed that the fluorescence signals associated with cdMMP-9 were gradually and significantly shifted from a mean of 22 in the error-prone library to 36 after R1, 84 after R2, 423 after R3 and finally reaching 1,063 after R4 (Fig. 3). The cdMMP-9 signal of R4 was dramatically higher than that of 3A2 wt or the library, suggesting FACS indeed enriched MMP-9 binders. Furthermore, the mean fluorescence on cdMMP14-Alexa647 decreased from 20 in the error-prone library to a background level of ~5 in R2–R4. These values were significantly less than the one associated with 3A2 (mean = 97), indicating that the competitive FACS successfully removed MMP-14 binders.

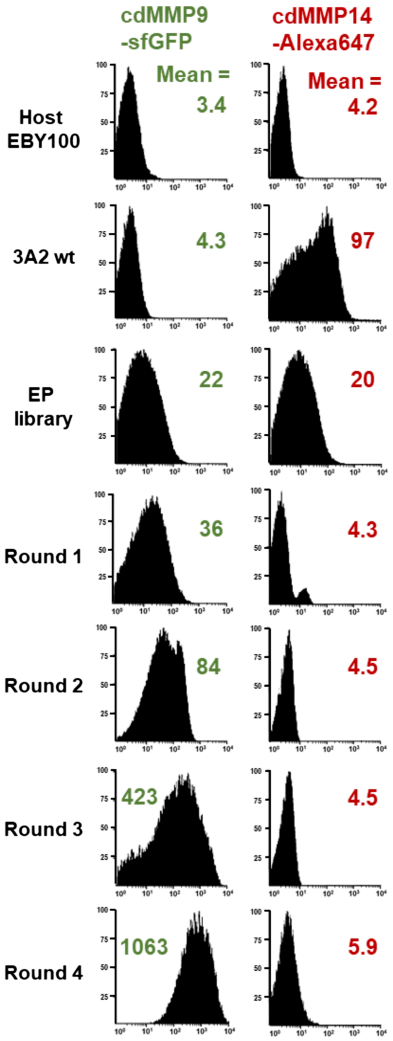

Figure 3. FACS analysis of cell populations before and after each round of sorting. For each sample, cells were stained with 400-nM cdMMP9-sfGFP and 400-nM cdMMP14-Alexa647. Cells displaying scFv 3A2 wt and host cells without scFv display were included as controls.

Monoclonal screening and identifying MMP-9 specific scFvs

After four rounds of screening, 20 randomly picked scFv clones were analyzed by monoclonal FACS. Their Q4 percentages, corresponding to cdMMP9-sfGFP positive cdMMP14-Alexa647 negative, were used to select the clones for further characterizations. Out of this pool of 20 candidates, 6 scFvs had a Q4 percentage greater than 90%, 13 were between 80% and 90% and the last clone had a Q4 percentage of 72%. As comparison, 3A2 and the error-prone library had Q4 percentages of 0.6% and 2.7%, respectively. More specifically, scFv clone 9C1 showed the highest cdMMP9-sfGFP fluorescence signal mean at 1,121, with other five clones (9C4, 9C10, 9C12, 9C17, and 9C20) showing signal means in the range of 500–900 (Fig. S1). These values were dramatically greater than that of 3A2 at 4.3. Furthermore, these six selected clones had their fluorescence signal means on cdMMP14-Alexa647 reduced from 97 of 3A2 to a background level of 4.4–6.5. Collectively, monoclonal FACS analysis indicated a clear shift of binding specificity from cdMMP-14 to cdMMP-9 for the isolated clones.

Genes of these six scFv clones were recovered for DNA sequencing. Results revealed that all of them were unique with most mutations scattered throughout scFv genes. As their specific mutations shown in Table 1, 9C1, 9C10, 9C12, 9C17, and 9C20 scFvs each had 2–4 amino acid mutations on their V_H and V_L. 9C4 was an exception, and had 12 mutations, with 5 single-site mutations and a continual mutation at CDR-H3 from L_{100i}VATPYGR$_{100p}$ to RSR-PRTGG. DNA sequence analysis revealed this octapeptide mutation was caused by a frameshift given by single nucleotide deletion in the middle of CDR-H3. A single nucleotide addition was also found close to the C-terminal of CDR-H3, to bring the open reading frame back.

MMP-9 inhibitory scFvs with high selectivity and stability

Isolated scFvs were sub-cloned into *E. coli* periplasmic expression vectors for production. Purified scFvs were tested for their binding affinities on cdMMP-9. As data shown in Table 1, 9C1 exhibited a K_D value of 29 nM ($k_{on} = 1.3 \times 10^5\ M^{-1}\ s^{-1}$, $k_{off} = 3.9 \times 10^{-3}\ s^{-1}$), 9C10 had a K_D of 34 nM ($k_{on} = 1.4 \times 10^5\ M^{-1}\ s^{-1}$, $k_{off} = 4.8 \times 10^{-3}\ s^{-1}$) and 9C17 had a K_D of 24 nM ($k_{on} = 4.2 \times 10^5\ M^{-1}\ s^{-1}$, $k_{off} = 1.0 \times 10^{-2}\ s^{-1}$), with the other three scFvs showing K_D between 54 and 130 nM. As expected, 3A2 scFv bound to cdMMP-9 very weakly with a K_D estimated larger than 5 μM. Next, the selectivity of isolated scFvs on cdMMP-9 over a panel of cdMMPs (-2/-12/-14) was tested by FRET inhibition assays using a general MMP substrate. In contrast to 3A2 showing its inhibition selectivity toward cdMMP-14, five isolated scFv mutants (9C1, 9C4, 9C10, 9C17, and 9C20) strongly preferred cdMMP-9 over cdMMP-2/-12/-14 (Fig. 4). The only exception was 9C12, which bi-specifically inhibited both cdMMP-9 and -12 with a similar strength. However, 9C12 exhibited a much steeper sigmoidal dose-response curve on cdMMP-9 than cdMMP-12, with calculated Hill coefficients of 2.5 and 1.0, respectively, suggesting a positively cooperative binding between 9C12 and cdMMP-9.

Inhibition potency K_Is were further calculated for quantitative comparisons (Table 1). For instance, 9C1 inhibited cdMMP-9 with a K_I of 120 nM, which was 22-fold stronger than its K_I on cdMMP-14 (2.6 μM). Taking K_Is of 3A2 on cdMMP-9/-14 (4.6 μM vs 40 nM) into account, our study flipped the inhibition selectivity on cdMMP-9 over -14 from 3A2's 1:155 to 9C1's 22:1, equivalent to a selectivity change of 2,500-folds. The other five isolated scFv mutants, compared to 3A2 scFv, also showed dramatic selectivity shifts of 690–4,500 folds from cdMMP-14 to cdMMP-9. Furthermore, although only cdMMP-14 was used for the counter-selection during our FACS, isolated scFvs also exhibited strong selectivity over cdMMP-2/-12, which were not used during screening. Taking cdMMP-2, a gelatinase sharing a high degree of homology with cdMMP-9 (Fig. 2, Table S1) as an example, isolated scFvs showed K_Is of 1.2–4.4 μM, which were in average 19-folds weaker than their K_Is on cdMMP-9. The bi-specificity of 9C12 on cdMMP-9 and -12 was confirmed by quantitative

Table 1. Identifying cdMMP-9 specific scFvs and their binding affinities, inhibition potencies and stabilities

scFv	Mutations		Affinity K_D (nM)		Inhibition potency K_I (nM)				Stability—% remaining after 12 h w/ 1-μM cdMMP-9
	VH	VL	cdMMP-9	cdMMP-2	cdMMP-9	cdMMP-12	cdMMP-14	Ratio -2 : -9 : -12 : -14	
3A2	-	-	>5,000	2,600	4,600	2,100	**40**	65 : 115 : 53 : 1	Not determined
9C1	A100kV	M4V	29	1,600	**120**	1,300	2,600	13 : 1 : 11 : 22	70
9C4	W36R/I69K/ N76D/L97P/ L_{100i}VATPYGR-> RSRPRTGGG	I21N	54	1,200	**170**	1,600	2,000	7 : 1 : 9 : 12	78
9C10	V37M/I51F/ S70G	F83S	34	3,700	**100**	1,300	1,600	37 : 1 : 13 : 16	96
9C12	M100sI	I75F/P94L	78	1,500	**91**	94	1,500	16 : 1 : 1 : 16	92
9C17	V63D	A51T	24	3,300	**150**	3,400	870	22 : 1 : 23 : 6	96
9C20	F27I/Y56H/ W100eR	-	126	4,400	**220**	4,400	8,500	20 : 1 : 20 : 39	98

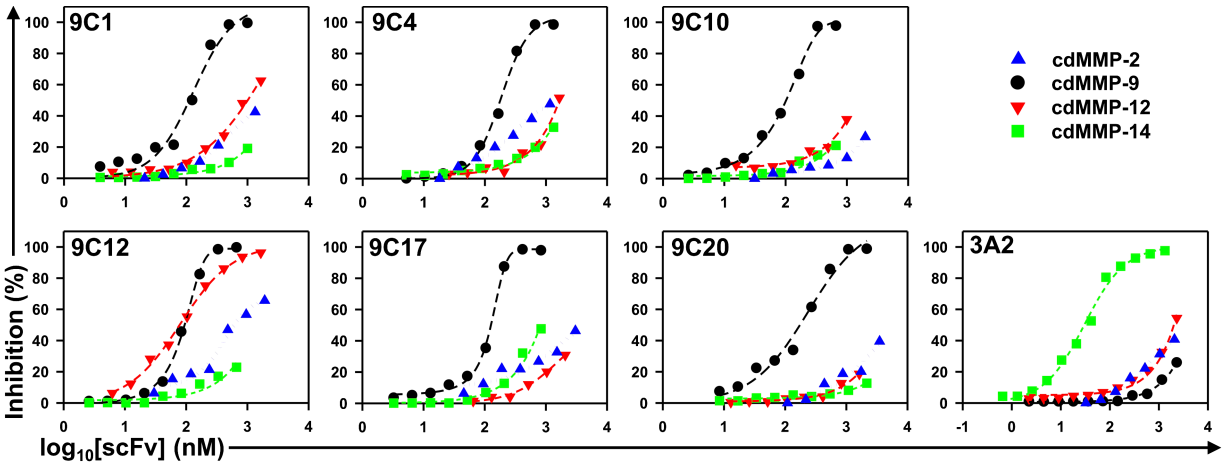

Figure 4. Inhibition of isolated scFvs on cdMMP-2/-9/-12/-14. The scFvs were serially diluted and reacted with 10-nM individual cdMMP and 1-μM M2350, an MMP general FRET peptide substrate. 3A2 scFv was tested as control.

analysis showing K_Is of 91 and 94 nM, respectively. Notably, 9C12 still retains its selectivity on cdMMP-9 over cdMMP-14 at a ratio of 23:1.

As standard mechanism biologic inhibitors of proteases tend to be slowly cleaved by the targeted proteases [44], proteolytic resistance is a desired pharmaceutical property of inhibitory antibodies. During FACS preparation and sorting, library cells were incubated with cdMMP9-sfGFP for extended periods of time. This treatment should bias the selection towards proteolytic resistant clones, as the vulnerable scFvs were cleaved by cdMMP-9 and the generated scFv truncations likely lost their binding affinities, which could be efficiently removed by FACS. To validate the stability of isolated clones, 1-μM purified scFvs were incubated with 1-μM cdMMP-9 at pH 7.5 37°C. After 3 and 12 h, samples were subjected to SDS-PAGE (Fig. S2). As densitometric analysis results shown in Fig. S3, on average only 2% of the scFvs were degraded after incubation for 3 h. And after 12-h incubation, 70% intact 9C1, 79% 9C4, and 92–99% of the other four scFvs remained, indicating a decent proteolytic stability.

Inhibition mechanism of MMP-9 specific scFv inhibitors

To understand their inhibition mechanism, kinetics of cdMMP-9 were measured in the presence of purified scFvs at different concentrations. As Lineweaver–Burke plots with scFv 9C1 show in Fig. 5A, when 9C1 concentration increased from 125 nM to 500 nM, the K_m significantly

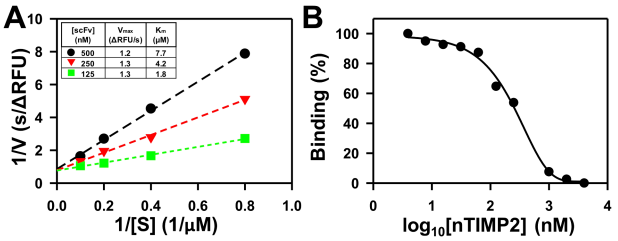

Figure 5. Inhibition mechanism of 9C1. (A) Lineweaver–Burke plots of cdMMP-9 in the presence of 125-, 250- and 500-nM scFv were developed. (B) Competitive ELISA with nTIMP-2.

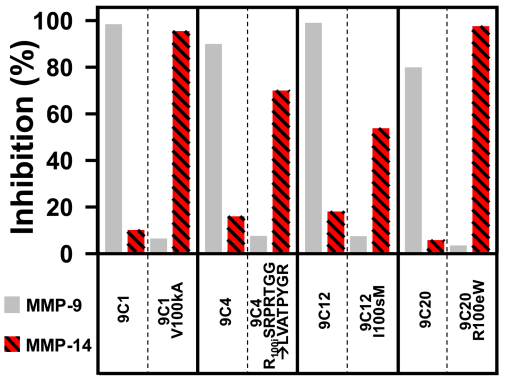

Figure 6. Paratope mutation studies of 9C1, 9C4, 9C12 and 9C20. The mutations in CDR-H3s were changed back to the amino acids of 3A2, and their inhibitory activities were tested. 500-nM scFvs and 10-nM cdMMP-9/-14 were used. Results were compared with inhibitory activities of 9C1, 9C4, 9C12 and 9C20 under the same assay conditions.

increased from 1.8 μM to 7.7 μM, while V_{max} remained unchanged (inset table of Fig. 5A), suggesting that 9C1 behaved as a classical competitive inhibitor. Similar assays were applied to the other five scFvs, and their results of unaltered V_{max} with increased K_m at increasing scFv concentrations indicated a competitive inhibition mode for all scFvs (Fig. S4A). To understand the binding landscape of these scFv competitive inhibitors, we performed competitive ELISA with N-terminal domain of TIMP-2. As the native inhibitor of MMP and ADAM family metalloproteinases, nTIMP-2 achieves its inhibitory function by directly binding to the active site in a manner similar to that of substrates. In the competitive ELISA, mixtures of a fixed amount of scFv with various concentrations of nTIMP-2 were incubated on a cdMMP-9 coated surface, then the scFvs captured by the immobilized cdMMP-9 were detected. As the sigmoidal curve shows in Fig. 5B, high concentrations of nTIMP-2 displaced scFv 9C1 on binding to cdMMP-9. Presumably, it suggested that the epitope of 9C1 was at least partially overlapped with that of nTIMP-2 and 9C1 directly targeted the substrate-binding cleft. Analysis of the other five scFvs indicated a similar competitive nature with nTIMP-2 on binding to cdMMP-9 (Fig. S4B). Notably, the behavior of competitive inhibition was also the characteristic of 3A2 wt [19], implying that altering the inhibition selectivity among protease family members by affinity maturation may retain the action mode of inhibition. Nevertheless, alternative possibilities of inhibitor induced conformational changes also exist. To fully distinguish whether these competitive inhibitors directly targeted the substrate-binding cleft or allosterically acted on an exosite, further investigations by epitope mapping and antibody-MMP complex structure determinations are needed.

Out of the six isolated cdMMP-9 specific scFvs, 9C1, 9C4, 9C12 and 9C20 had mutations within their CDR-H3s. We hypothesized that these CDR-H3 mutations provided the key interactions responsible for their switched inhibition selectivity toward cdMMP-9 over cdMMP-14. To test this hypothesis, we performed site-directed mutagenesis on paratopes of these four scFvs, by changing their CDR-H3 mutations back to the residues of 3A2 wt, and compared their inhibition activities, at 500 nM scFv, on 10 nM cdMMP-9 or cdMMP-14. Unlike 9C1 scFv that showed selective inhibition toward cdMMP-9 (98% inhibition) over cdMMP-14 (10% inhibition), its reverse mutant 9C1 $V_{100k}A$ reduced its inhibitory activity on cdMMP-9 to 8% while regaining its inhibition on cdMMP-14 to 95% (Fig. 6). These results, together with the observation that $A_{100k}V$ is the only mutation on 9C1 V_H domain, suggested that 100k was a critical position for determining selectivity—Val at 100k led to binding/inhibition of cdMMP-9 while Ala at 100k led to cdMMP-14.

Surface modeling shows that the extruded F260 residue on cdMMP-14 versus the relatively flat M422 on cdMMP-9 is a major discrepancy between these cdMMPs within their active clefts (Fig. 1B). Presumably, this 100k position on 9C1 could directly interact with F260/M422 side chains on cdMMP-14/-9. 9C1's Val_{100k} could introduce spatial constraints with cdMMP-14's F260, while occupying the vacancy cdMMP-9's M422 leaves. Similarly, 9C4, 9C12, and 9C20 paratope reverse mutants showed inhibition reduction toward cdMMP-9 with restoration of their inhibition activity on cdMMP-14, however to different degrees. For example, 9C12 $I_{100s}M$ only restored 50% inhibition on cdMMP-14, suggesting that other mutated residues on 9C12 also contributed to the selectivity switch. Collectively, enzyme kinetics, competitive ELISA, and paratope mutagenesis studies suggested that isolated MMP-9 specific scFvs were competitive inhibitors having epitope overlapped with TIMP-2 and their key residues in the CDR-H3 region significantly contributed to their inhibition selectivity.

Affinity and selectivity matured cdMMP-14 specific scFvs

After three rounds of FACS with selection on cdMMP14-Alexa647 and counter-selection on cdMMP9-sfGFP, three unique scFv clones with MMP-14 specificity were identified (Table S2). On monoclonal FACS, clones 14C4, 14C5, and 14C10 showed 5.3–6.6-fold increases of fluorescence signals on cdMMP14-Alexa647 compared to that of 3A2, while retaining low signals on cdMMP9-sfGFP at the background level. BLItz analysis on cdMMP-14 revealed enhanced affinity (K_D) compared to 3A2 scFv's at 25 nM: 14C4 at 5.9 nM ($k_{on} = 4.4 \times 10^6$ M^{-1} s^{-1}, $k_{off} = 2.6 \times 10^{-2}$ s^{-1}), 14C5 at 1.9 nM ($k_{on} = 2.2 \times 10^7$ M^{-1} s^{-1}, $k_{off} = 4.2 \times 10^{-2}$ s^{-1}), and 14C10 at 2.2 nM ($k_{on} = 9.8 \times 10^6$ M^{-1} s^{-1}, $k_{off} = 2.2$

$\times 10^{-2}$ s^{-1}). Inhibition potency on cdMMP-14 was also improved to 6.1–23 nM from 39 nM of 3A2. Similarly to 3A2, isolated scFvs exhibited weak inhibition on cdMMP-9 even at 1-μM scFv concentration. *In vitro* stability tests by incubating 1-μM scFv with 1-μM cdMMP-14 at 37°C pH 7.5 for 12 h indicated that isolated mutants had 82–95% intact scFv remaining, in contrast with 3A2 wt, which showed 96% degradation, suggesting significant improvements on proteolytic stability (Fig. S5).

DISCUSSION

At least 23 MMP family members have been identified in the human genome. Although different in their domain arrangements and substrate preferences, the catalytic subunits of all MMPs share high degrees of sequence similarity and protein folding. Many MMPs play important, albeit frequently paradoxical, roles in multiple pathologies including cancer [45], neuropathic pain [33], chronic wounds [46], cardiovascular alterations [47] and infectious diseases [48]. MMPs together with their native regulatory inhibitors (TIMP1–4) and associated substrates form a complicated proteolytic network. It is an urgent need to develop selective and efficient inhibitors of individual MMPs for both disease therapies and biomedical research. In fact, the lack of highly specific inhibitors is a major hurdle for understanding proteolytic degradome. For instance, during tumor progression, it remains rather elusive when, where and how much certain MMPs exhibit their proteolytic activities. Using MMP-specific mAbs and their dye/radioisotope conjugations as imaging probes will enable us to narrow down the location and the time frame of particular proteolytic action. Specifically blocking individual MMP by inhibitory mAbs will further advance our understandings on the molecular mechanisms by which diseases develop, e.g. how cancer cells migrate through extracellular matrix. One application is to identify the dominate proteases present in tumor microenvironments for the development of prodrug therapeutics, which are activated by the proteolytic cleavage of certain protease(s).

Current methods for protease inhibitory mAb discovery usually start with the isolation of target-specific binders, followed by functional screening to identify inhibitors. However, isolated mAbs, which specifically bind, do not necessarily function as inhibitors. Recent developments on antigen mimicry design [26], antibody library customization [19], and functional selections [20] have greatly advanced the field. This study developed a novel and complementary approach able to switch the inhibition selectivity among closely related protease family members. More specifically, such selectivity change was achieved by performing FACS selection and counter-selection simultaneously, a similar method has been recently applied for engineering MMP-specific TIMPs [49]. As proof of concept, we converted an MMP-14 inhibitor to a panel of MMP-9 inhibitors with 690–4,500-fold selectivity shift. Notably, the first round sorting without depletion of MMP-14 positive cells generated two cell populations on cdMMP14-Alexa647 spectrum: a major peak at 4.2 and a minor peak at 18 (Fig. 3), suggesting there could be a small fraction of cells binding both MMP-14 and MMP-9. Therefore, this method can be applied to generate not only monospecific inhibitors to single MMPs but also inhibitors with bi- or oligo-specificity. During FACS, antibody library cells were incubated with MMP(s) for extensive periods of time. As a result, all the isolated antibody mutants exhibited excellent proteolytic stability (Figs S2, S3, S5).

The mAbs inhibiting numerous biomedically important proteases, such as MT-SP1 (membrane type serine protease) [27], plasma kallikrein [28], factor Xa [29], BACE-1 (beta-secretase 1) [31] etc, have been identified. Because most of these proteases are present in families, the method described here can be applied to convert these isolated inhibitory mAbs to inhibit other members of the associated families. In summary, the advantages of this study over current methods of protease inhibitory antibody include (1) its straightforwardness without immunization or phage panning; (2) high proteolytic stability of isolated clones; (3) potential to generate mono-, bi-, and oligo-specific inhibitors; (4) its quantitative and high-throughput nature; and (5) other than applications for mAb inhibitors targeting MMPs, we believe the methodology demonstrated here can be particularly useful for the generation of inhibitory mAbs targeting many other proteases of biomedical importance.

SUPPLEMENTARY DATA

Supplementary Data are available at *ABT* online.

AUTHOR CONTRIBUTIONS

T.L. and X.G.: design research, analyze data and write manuscript. T.L., A.R., C.B., Z.M., H.P. and R.S.: perform experiments.

FUNDING

This work was supported by the National Institutes of Health 1R01GM115672 and Faculty Early Career Development Program of National Science Foundation 1453645.

ACKNOWLEDGMENTS

We thank UCR Graduate Research Mentorship and Dissertation Year Program fellowships that partially support T.L. and UCR Sophomore STEM Success Award to A.R.

REFERENCES

1. Docherty, AJ, Crabbe, T, O'Connell, JP et al. Proteases as drug targets. *Biochem Soc Symp* 2003; 70: 147–61.
2. Turk, B. Targeting proteases: successes, failures and future prospects. *Nat Rev Drug Discov* 2006; 5: 785–99.
3. López-Otín, C, Judith, S. Bond proteases: multifunctional enzymes in life and disease. *J Biol Chem* 2008; 283: 30433–7.
4. Cudic, M, Fields, GB. Extracellular proteases as targets for drug development. *Curr Protein Pept Sci* 2009; 10: 297–307.
5. Drag, M, Salvesen, GS. Emerging principles in protease-based drug discovery. *Nat Rev Drug Discov* 2010; 9: 690–701.
6. López-Otín, C, Matrisian, L. Emerging roles of proteases in tumour suppression. *Nat Rev Cancer* 2007; 7: 800–8.

7. Koblinski, JE, Ahram, M, Sloane, BF. Unraveling the role of proteases in cancer. *Clin Chim Acta* 2000; 291: 113–35.
8. Greenbaum, DC, Baruch, A, Grainger, M et al. A role for the protease falcipain 1 in host cell invasion by the human malaria parasite. *Science.* 2002; 298: 2002–6.
9. Hopp, CS, Bennett, BL, Mishra, S et al. Deletion of the rodent malaria ortholog for falcipain-1 highlights differences between hepatic and blood stage merozoites. *PLoS Pathog* 2017; 13: e1006586.
10. McCarty, S, Percival, S. Proteases and delayed wound healing. *Adv Wound Care* 2013; 2: 438–47.
11. Walker, CP, Royston, D. Thrombin generation and its inhibition: a review of the scientific basis and mechanism of action of anticoagulant therapies. *Br J Anaesth* 2002; 88: 848–63.
12. Kaplan, AP. Enzymatic pathways in the pathogenesis of hereditary angioedema: the role of C1 inhibitor therapy. *J Allergy Clin Immunol* 2010; 126: 918–25.
13. Puente, XS, Sánchez, LM, Overall, CM et al. Human and mouse proteases: a comparative genomic approach. *Nat Rev Genet* 2003; 4: 544–58.
14. Tallant, C, Marrero, A, Gomis-Rüth, FX. Matrix metalloproteinases: fold and function of their catalytic domains. *Biochim Biophys Acta.* 2010; 1803: 20–8.
15. Lee, M, Fridman, R, Mobashery, S. Extracellular proteases as targets for treatment of cancer metastases. *Chem Soc Rev* 2004; 33: 401–9.
16. Kessenbrock, K, Plaks, V, Werb, Z. Matrix metalloproteinases: regulators of the tumor microenvironment. *Cell* 2010; 141: 52–67.
17. Overall, CM, Kleifeld, O. Towards third generation matrix metalloproteinase inhibitors for cancer therapy. *Br J Cancer* 2006; 94: 941–6.
18. Zucker, S, Cao, J. Selective matrix metalloproteinase (MMP) inhibitors in cancer therapy Ready for prime time? *Cancer Biol Ther* 2009; 8: 2371–3.
19. Nam, DH, Rodriguez, C, Remacle, A et al. Active-site MMP-selective antibody inhibitors discovered from convex paratope synthetic libraries. *Proc Natl Acad Sci U S A.* 2016; 113: 14970–5.
20. Nam, DH, Fang, K, Rodriguez, C et al. Generation of inhibitory monoclonal antibodies targeting matrix metalloproteinase-14 by motif grafting and CDR optimization. *Protein Eng Des Sel* 2017; 30: 113–8.
21. Lopez, T, Nam, DH, Kaihara, E et al. Identification of highly selective MMP-14 inhibitory fabs by deep sequencing. *Biotechnol Bioeng* 2017; 114: 1140–50.
22. De Genst E, Silence K, Decanniere K, et al. (2006) Molecular basis for the preferential cleft recognition by dromedary heavy-chain antibodies. *Proc Natl Acad Sci U S A* 103: 4586–91.
23. Farady, CJ, Sun, J, Darragh, MR et al. The mechanism of inhibition of antibody-based inhibitors of membrane-type serine protease 1 (MT-SP1). *J Mol Biol* 2007; 369: 1041–51.
24. Wu, Y, Eigenbrot, C, Liang, WC et al. Structural insight into distinct mechanisms of protease inhibition by antibodies. *Proc Natl Acad Sci U S A* 2007; 104: 19784–9.
25. Devy, L et al. Selective inhibition of matrix metalloproteinase-14 blocks tumor growth, invasion, and angiogenesis. *Cancer Res* 2009; 69: 1517–26.
26. Sela-Passwell, N, Kikkeri, R, Dym, O et al. Antibodies targeting the catalytic zinc complex of activated matrix metalloproteinases show therapeutic potential. *Nat Med* 2012; 18: 143–7.
27. Schneider, EL, Lee, MS, Baharuddin, A et al. A reverse binding motif that contributes to specific protease inhibition by antibodies. *J Mol Biol* 2012; 415: 699–715.
28. Kenniston, JA, Faucette, RR, Martik, D et al. Inhibition of plasma kallikrein by a highly specific active site blocking antibody. *J Biol Chem* 2014; 289: 23596–608.
29. David, T, Kim, YC, Ely, LK et al. Factor XIa–specific IgG and a reversal agent to probe factor XI function in thrombosis and hemostasis. *Sci Transl Med* 2016; 8: 353ra112.
30. Ling, B, Watt, K, Banerjee, B et al. A novel immunotherapy targeting MMP-14 limits hypoxia, immune suppression and metastasis in triple-negative breast cancer models. *Oncotarget* 2017; 8: 58372–85.
31. Atwal, JK, Chen, Y, Chiu, C et al. A therapeutic antibody targeting BACE1 inhibits amyloid-β production in vivo. *Sci Transl Med* 2011; 3: 84ra43.
32. Lopez T, Chen C, Ramirez A, et al. Epitope specific affinity maturation improved stability of potent protease inhibitory antibodies. *Biotechnol Bioeng*, doi: 10.1002/bit.26814. [Epub ahead of print]
33. Ji, RR, Xu, ZZ, Gao, YJ. Emerging targets in neuroinflammation-driven chronic pain. *Nat Rev Drug Discov* 2014; 13: 533–48.
34. Levina, M, Weiss, GA. Optimizing the affinity and specificity of proteins with molecular display. *Mol Biosyst* 2016; 2: 49–57.
35. Eaton, B, Gold, L, Zichi, D. Let's get specific: the relationship between specificity and affinity. *Chem Biol* 1995; 2: 633–8.
36. Yin, J, Beuscher, A, Andryski, S et al. Structural plasticity and the evolution of antibody affinity and specificity. *J Mol Biol* 2003; 330: 651–6.
37. Nam, DH, Ge, X. Direct production of functional matrix metalloproteinase-14 without refolding or activation and its application for in vitro inhibition assays. *Biotechnol Bioeng* 2016; 113: 717–23.
38. Hayhurst, A, Happe, S, Mabry, R et al. Isolation and expression of recombinant antibody fragments to the biological warfare pathogen Brucella melitensis. *J Immunol Methods* 2003; 276: 185–96.
39. Brandt, RB, Laux, JE, Yates, SW. Calculation of inhibitor Ki and inhibitor type from the concentration of inhibitor for 50% inhibition for Michaelis–Menten enzymes. *Biochem Med Metab Biol* 1987; 37: 344–9.
40. Goldenzweig, A, Goldsmith, M, Hill, S et al. Automated structure- and sequence-based design of proteins for high bacterial expression and stability. *Mol Cell* 2016; 63: 337–46.
41. Lee, KB, Nam, DH, Nuhn, JA et al. Direct expression of active human tissue inhibitors of metalloproteinases by periplasmic secretion in *Escherichia coli*. *Microb Cell Fact* 2017; 16: 73.
42. Boder, ET, Wittrup, KD. Yeast surface display for screening combinatorial polypeptide libraries. *Nat Biotechnol* 1999; 15: 553–37.
43. Pédelacq, JD, Cabantous, S, Tran, T et al. Engineering and characterization of a superfolder green fluorescent protein. *Nat Biotechnol* 2006; 24: 79–88.
44. Farady, CJ, Craik, CS. Mechanisms of macromolecular protease inhibitors. *Chembiochem* 2010; 11: 2341–6.
45. Gialeli, C, Theocharis, AD, Karamanos, NK. Roles of matrix metalloproteinases in cancer progression and their pharmacological targeting. *FEBS J* 2011; 278: 16–27.
46. Cook, H, Stephens, P, Davies, KJ et al. Defective extracellular matrix reorganization by chronic wound fibroblasts is associated with alterations in TIMP-1, TIMP-2, and MMP-2 activity. *J Investig Dermatol* 2000; 115: 225–33.
47. Castro, MM, Tanus-Santos, JE. Inhibition of matrix metalloproteinases (MMPs) as a potential strategy to ameliorate hypertension-induced cardiovascular alterations. *Curr Drug Targets* 2013; 14: 335–43.
48. Elkington, PTG, O'Kane, CM, Friedland, JS. The paradox of matrix metalloproteinases in infectious disease. *Clin Exp Immunol* 2005; 142: 12–20.
49. Shirian, J, Arkadash, V, Cohen, I et al. Converting a broad matrix metalloproteinase family inhibitor into a specific inhibitor of MMP-9 and MMP-14. *FEBS Lett* 2018; 592: 1122–34.